The Mechanism of Electrochemical Reduction of Hydrogen Peroxide on Silver Nanoparticles

Xiaosheng Cai,[1] Eden E. L. Tanner,[2] Chuhong Lin,[2] Kamonwad Ngamchuea,[2] John S. Foord,[1] and Richard G. Compton[*2]

[1]Department of Chemistry, Chemistry Research Laboratory, University of Oxford, Mansfield Road, Oxford, OX1 3TA, United Kingdom.

[2]Department of Chemistry, Physical and Theoretical Chemistry Laboratory, University of Oxford, South Parks Road, Oxford OX1 3QZ, United Kingdom

*Corresponding Author:

Emails: richard.compton@chem.ox.ac.uk

Phone: +44(0) 1865 275957

Fax: +44 (0) 1865 275410

Abstract

The reduction of hydrogen peroxide on a silver nanoparticle modified boron doped diamond electrode in a neutral solution is shown to proceed through a CE mechanism. Hydrogen peroxide undergoes a disproportionation reaction to form oxygen (and water) on the silver surface, creating a diffusion layer of oxygen, which, at a sufficiently biased electrode, is then reduced to hydrogen peroxide. Voltammetry and a full mechanistic simulation are undertaken to confirm the mechanism, showing at short times a dependence of the reductive signal on waiting time prior to voltammetric analysis reflecting the extent of the disproportionation step which occurs prior to voltammetric analysis.

Keywords: hydrogen peroxide reduction, mechanism, nanoparticle modified electrodes, silver

Introduction

The reduction of hydrogen peroxide (H_2O_2) on silver electrodes has been extensively studied, with over 159 papers published on the subject since 2005, when Welch *et al.*[1] reported the electrochemical detection of hydrogen peroxide using a silver nanoparticle modified glassy carbon electrode. A review of hydrogen peroxide detection on metal nanoparticles was published in 2013 by Chen *et al.*,[2] and in the last two years alone a number of papers have been published on the subject,[3, 4] including investigating the effect of modifying the nanoparticles,[5, 6] the pH[7, 8] and the carbon electrode.[9-14]

Determining the mechanism of this process is an open question with high interest due to the fact that different mechanisms operate depending on the context (for example the electrode material and pH). The most commonly proposed mechanism in acidic and neutral conditions is usually *assumed* to be:

$$H_2O_2 + H^+ + e^- \rightarrow OH_{ads} + H_2O \quad (1)$$

$$H^+ + OH_{ads} + e^- \rightarrow H_2O \quad (2)$$

The vast majority of studies investigating hydrogen peroxide reduction (including those cited above) are analytically or applications focused and presume the above process holds true. Understanding the mechanism operating is critical to optimising any application that relies on hydrogen peroxide reduction.

In particular, the possible role of oxygen reduction in this process has not yet been examined, despite the fact that oxygen reduction on silver in neutral aqueous media, as studied in detail by Neumann *et al.*,[15] has been shown to proceed through a 2 electron reduction to hydrogen peroxide, and that the latter is known to disproportionate on silver.

Consequently in this paper we consider an alternative mechanism for hydrogen peroxide reduction – a CE process involving an initial disproportionation of the hydrogen peroxide into oxygen that is followed by an electron transfer:

$$H_2O_2 \rightarrow 1/2O_2 + H_2O \quad (3)$$

$$O_2 + 2e^- + 2H^+ \rightarrow H_2O_2 \quad (4)$$

This mechanism is herein investigated in the context of silver nanoparticle modified boron doped diamond electrodes (BDDE) and supported by simulations, providing strong evidence that a CE reaction with an oxygen reduction step is the mechanism operating in neutral pH for the reduction of hydrogen peroxide on silver nanoparticle modified electrodes.

Theory and Simulation

The CE electrode reaction under consideration contains two parts. Before applying the potential to the electrode, the hydrogen peroxide in the solution reacts to form oxygen at the surface of the silver catalyst:

$$\mathrm{H_2O_2} \xrightarrow{k_{\mathrm{het}}} \mathrm{H_2\,O} + \frac{1}{2}\mathrm{O_2} \qquad (3)$$

where k_{het} is the heterogeneous disproportionation rate constant (m s^{-1}). We assume that the oxidation of the hydrogen peroxide occurs at a time t = 0, corresponding to insertion of the electrode into the solution. Subsequently a reductive voltammetric scan is initiated at a time t_{het} (s) leading to the reduction of the product oxygen:

$$\mathrm{O_2} + 2e^- + 2\mathrm{H^+} \xrightarrow{k_0;\alpha} \mathrm{H_2O_2} \qquad (4)$$

where k_0 is the electron transfer rate constant (m s^{-1}) and α is the transfer coefficient.[16, 17] Note H_2O_2 is assumed not to be active at the potentials required for the reduction of O_2.

Assuming that there is enough amount of electrolyte in the solution and the experimental time is rather short, the influence of the migration and convection can be ignored.[18, 19] So that the change of the concentration in the solution is only driven by diffusion. As the electrode used in the experiments reported below is relatively large compared to the diffusion layer, and the coverages of nanoparticles used are approximately mono-layers,[20-23] we only need to consider diffusion that is perpendicular to the plane of the electrode surface.[24] Therefore, the three-dimensional electrode system can be simplified to a one-dimension problem. Fick's second law for the one-dimensional diffusion equation is:[25]

$$\frac{\partial c(t,x)}{\partial t} = D\frac{\partial^2 c(t,x)}{\partial x^2} \qquad (5)$$

where c (t, x) is the concentration (mol m^{-3}, mM), calculated as a function of the reaction time t (s) and the space distance x (m). x represents the dimension perpendicular to the electrode. D is the diffusion coefficient (m^2 s^{-1}).

During the heterogeneous disproportionation reaction ($t < t_{wait}$, t_{wait} is the time of waiting before implementing the linear potential sweep to the electrode), the reaction rate equations of H_2O_2 and O_2 at the electrode surface are expressed as:

$$D_{H_2O_2}\frac{\partial c_{H_2O_2}(t,x)}{\partial x}\Big|_{x=0} = k_{het}c_{H_2O_2}(t, x=0) \qquad (6)$$

$$D_{O_2}\frac{\partial c_{O_2}(t,x)}{\partial x}\Big|_{x=0} = -\frac{1}{2}k_{het}c_{H_2O_2}(t, x=0) \qquad (7)$$

x = 0 corresponds to the electrode surface where the reactions occur. After the electrochemical reaction starts ($t > t_{wait}$), the rate equations change to:

$$D_{H_2O_2}\left.\frac{\partial c_{H_2O_2}(t,x)}{\partial x}\right|_{x=0} = k_{het}c_{H_2O_2}(t,x=0) - k_0'\exp\left(\frac{-\alpha F(E-E_f)}{RT}\right)c_{O_2}(t,x=0) \quad (8)$$

$$D_{O_2}\left.\frac{\partial c_{O_2}(t,x)}{\partial x}\right|_{x=0} = -\frac{1}{2}k_{het}c_{H_2O_2}(t,x=0) + k_0'\exp\left(\frac{-\alpha F(E-E_f)}{RT}\right)c_{O_2}(t,x=0) \quad (9)$$

where E is the applied electrode potential (V), E_f is the formal potential of redox couple H_2O_2/O_2, F is the Faraday constant (96485 C mol^{-1}), T is the room temperature (298 K), and R is the gas constant (8.314 J·mol^{-1}·K^{-1}). The electron transfer is described by the Butler-Volmer equation,[26, 27] assuming that the electron transfer is fully irreversible and k_0' is the effective standard electron transfer rate constant. To simulate the cyclic voltammetry applied in the experiment, the applied potential in the potential window [E_{ini}, E_{rev}] is expressed as a function of electrochemical reaction time t_{el} ($t_{el} = t - t_{wait}$) and the scan rate v (V s^{-1}):

$$E = \begin{cases} E_{ini} - vt_{el}, & t_{el} \le \frac{|E_{ini}-E_{rev}|}{v} \\ E_{rev} + v\left(t_{el} - \frac{|E_{ini}-E_{rev}|}{v}\right), & t_{el} > \frac{|E_{ini}-E_{rev}|}{v} \end{cases} \quad (10)$$

By solving the diffusion equation (Eqn.5) with the boundary conditions (Eqn.6-9), the concentration functions of H_2O_2 and O_2 can be derived. Therefore, the current I (A) measured at the electrode can be calculated from:

$$I = 2FSD_{O_2}\left.\frac{\partial c_{O_2}(t,x)}{\partial x}\right|_{x=0} \quad (11)$$

where S refers to the surface area of the electrode.

The resulting problem was solved numerically by means of the LU decomposition method, the details of which can be found in the literature.[24] The simulation programme was written in Matlab R2017a and performed using an Intel(R) Xeon(R) 3.60G CPU.

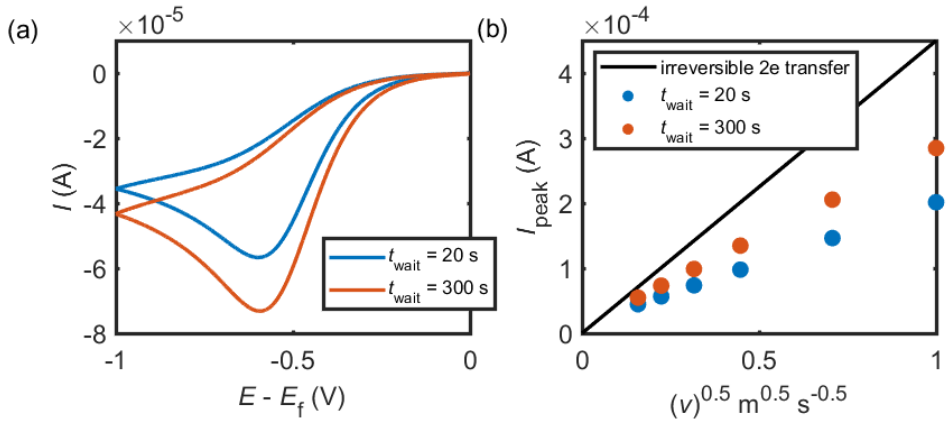

Figure 1 (a) Simulated cyclic voltammograms based on the theoretical model with a waiting time of 20s (the blue line) and 300 s (the red line); (b) Scan rate dependence of the peak currents. The black line is the calculated peak current for an irreversible two electron transfer reaction. Blue and red marks correspond to the simulation of 20 s and 300 s waiting times.

Figure 1 shows two example cyclic voltammograms and the corresponding scan rate dependence simulated from the above model. The disproportionation rate constant of hydrogen peroxide decomposition at the electrode is set to be 10^{-5} m s^{-1} (see below); the initial concentration of hydrogen peroxide is 1.0 mM; the diffusion coefficients of hydrogen peroxide and oxygen are found in the literature to be 1.43 x 10^{-9} and 1.96 x 10^{-9} m^2 s^{-1} in room temperature, respectively; [28-30] as oxygen reduction reaction is irreversible, the effective electron transfer k_0 is set to be 10^{-7} m s^{-1}, the transfer coefficient is 0.3 and each oxygen transfers two electrons during the reduction. In Figure 1a, the waiting times before commencing the linear potential sweep to the electrode t_{wait} are set to be 20 s (the blue line) and 300 s (the red line). The scan rate is 0.05 V s^{-1} in Figure 1a. The voltammograms of 20s and 300s t_{wait} have similar waveshapes but a longer t_{wait} leads to a much larger reaction current. In Figure 1b, the peak currents of 20s and 300s t_{wait} simulated with various scan rates

are compared with the case of irreversible two-electron transfer reaction. The peak current for an irreversible *n* electron transfer is calculated from the Randles-Ševčík equation[31] and shown by the black line in Figure 1b:

$$i_p = 2.99 \times 10^5 SD^{0.5} Cv^{0.5} n(n' + \alpha)^{0.5} \quad (12)$$

where *v* is the scan rate, *C* is the concentration of the reactant, *D* is the diffusion coefficient of the reactant, *n* is the electrons transferred corresponding to one reactant (*n* = 2), *n'* is the electron transferred before the rate-determining step (we infer *n*' = 0). From Figure 1b, it is found that for fast scan rates, the peak current based on the CE mechanism deviates from the Randles-Ševčík equation for a simple two-electron transfer reaction. This is because that in a CE reaction, the preceding chemical step sets up a reaction layer adjacent to the electrode surface where the redox species is generated for the following electrochemical reaction. At high scan rate, when the chemical reaction rate is slower than the diffusion speed, the reaction is controlled by the preceding chemical step and the current is smaller than the diffusion-limited value as predicted in Eqn. 12.

Figure 2 are the concentration profiles of O_2 related to the two reactions in Figure 1 as a function of the reaction time and the space distance. Figure 2a and 2b are the concentration profiles with 20 s and 300 s t_{wait}, respectively. To show the concentration variation clearly, each concentration profile is divided into two parts: the left part corresponds to the heterogeneous disproportionation reaction of hydrogen peroxide, where a layer of oxygen is generated adjacent to the electrode surface (*x* = 0), and the right part is the time during the cyclic voltammetry, where the generated oxygen is reduced at the electrode. In the time period of the heterogeneous disproportionation reaction, the layer of generated O_2 of the 300s t_{wait} in Figure 2b is broader than that of the 20s t_{wait}, reflecting on the larger reaction current of the 300s t_{wait} in Figure 1a.

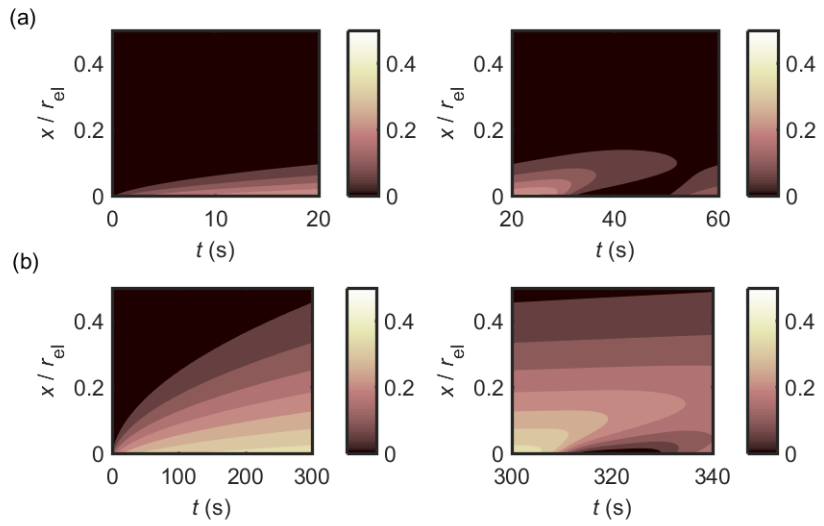

Figure 2 (a) Concentration profile of O_2 with 20 s waiting time; (b) Concentration profile of O_2 with 300 s waiting time. The concentration profile corresponds to the cyclic voltammograms in Figure 1a.

Experimental

Chemical reagents

The chemical reagents monosodium phosphate (NaH_2PO_4, ≥ 99.0%), disodium phosphate (Na_2HPO_4, ≥ 99.0%) and silver nanoparticles (AgNPs) dispersion were purchased from Sigma-Aldrich. The AgNPs with a diameter of 10 nm and concentration of 0.02 mg/mL were capped by sodium citrate (as supplied). The transmission electron microscopy image can be found from the website[32] of AgNPs product, confirming the presence of the nanoparticles. Hydrogen peroxide was obtained from Fisher Scientific International, Inc. All the reagents were used as received without any further purification. All solutions were prepared with ultrapure water (18.2 MΩ cm at 25 ^{o}C, Millipore, MA, USA)

Apparatus and electrochemical measurements

Electrochemical experiments were conducted with an Autolab PGSTAT128N potentiostat (Metrohm Autolab, Utrecht, Netherlands) and NOVA software. A three-electrode configuration was used consisting of a platinum (Pt) coil counter electrode and a Ag/AgCl reference electrode along with a boron-doped-diamond working electrode described below. A 0.1 M phosphate buffer solution (PBS, pH = 7.2) was used as the electrolyte for all experiments. Degassed solutions were bubbled with N_2 for 15 min, whilst oxygenated solutions were saturated with compressed air.

Electrode modification

The boron-doped-diamond wafer (Element Six Co.) with a boron doping concentration of ~ 5 × 10^{20} atoms cm^{-3} was used as the working electrode, and mounted in a home-made polytetrafluoroethylene (PTFE) holder as previously described[33] with a circular area of 0.37 cm^2 exposed to the electrolyte. Prior to each use, the boron-doped-diamond electrode was polished using alumina powder (Buehler, MicroPolish II) in the particle size sequence of 1 µm, 0.3 µm and 0.05 µm and diamond suspension (Buehler, MetaDi) in the size of 9 µm, 1 µm and 0.1 µm on lapping pads to ensure a clean surface.[34] To modify the BDDE, 100 µL of AgNPs dispersion was drop-cast onto the BDDE surface and allowed to dry to form the electrode herein referred to as AgNPs-BDDE. The surface morphology of the silver-modified BDDE was characterized by a Hitachi S-4300 field emission scanning electron microscopy (SEM) with a 20 kV acceleration voltage.

Results and Discussion

This section outlines the successful modification of a boron-doped-diamond electrode with silver nanoparticles, followed by a report of the voltammetry in the presence (and absence) of hydrogen peroxide and oxygen. A full mechanistic simulation is used to interpret the experimental voltammetry.

Under monolayer conditions, the diffusion layers of neighbouring AgNPs overlap heavily and consequently a monolayer coverage of nanoparticles will lead to a voltammetric response corresponding closely to 1D linear diffusion to the geometric area of the substrate.[20] Low coverage results in the local change of mass transport[35] while high coverage leads to aggregation and porosity.[36, 37] Therefore in this work a monolayer coverage is only considered to avoid introducing a further variable so as to focus on the H_2O_2 reduction mechanism. A boron-doped-diamond electrode was modified by placing 100 µL of a suspension containing 0.02 mg/mL 10 nm (diameter) silver nanoparticles (corresponding to 3.6×10^{11} nanoparticles, or *ca.* one monolayer coverage) onto the surface and allowing it to dry. The modified electrode was then characterised by scanning electron microscopy. Figure S1 shows an SEM image of silver modified BDDE. The particles are dispersed over the surface, demonstrating the successful modification of the electrode.

The modified electrode was then immersed for *ca.* 15 minutes in a degassed solution containing PBS buffer and increasing concentrations (0 – 19.2 mM) of hydrogen peroxide. A cyclic voltammogram (CV) was recorded by sweeping the potential from 0.0 V to -1.0 V vs Ag/AgCl at a scan rate of 0.05 V s^{-1} (Figure 3). In the presence of hydrogen peroxide, a peak appears on the forward scan at *ca.* - 0.6 – -0.9 V vs Ag/AgCl (with a peak potential of -0.6 V in concentrations ≤ 1.2 mM), and the reductive peak current increases linearly (see Figure 3c) with the hydrogen peroxide concentration.

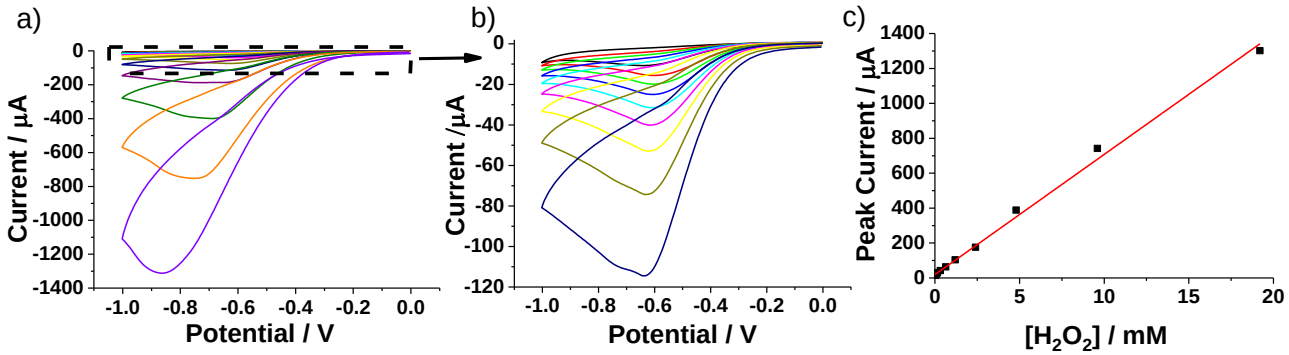

Figure 3. CVs of AgNPs-BDDE measured after ca. 15 minutes immersion in N_2-saturated PBS with H_2O_2 at a concentration of a) 0 mM (black), 0.01 mM (red), 0.02 mM (green), 0.04 mM (blue), 0.08 mM (cyan), 0.16 mM (magenta), 0.32 mM (yellow), 0.64 mM (dark yellow), 1.2 mM (navy), 2.4 mM (purple), 4.8 mM (olive), 9.6 mM (orange), and 19.2 mM (violet). b) is the zoomed-in area for lower H_2O_2 concentrations, c) is the peak current (baseline corrected) plotted against the hydrogen peroxide concentration, with R^2 = 0.996.

Having established the response of AgNPs-BDDE in the presence of hydrogen peroxide, further analysis of the voltammetry was performed in order to understand the electron transfer process. Tafel analysis was performed on the voltammograms (averaging data from 3 experiments at each concentration, shown in Figure S2), with the slope and the corresponding transfer coefficient α, being reported in Table S1. The average α value was calculated to be 0.26 ± 0.04 across all concentrations.

Using the transfer coefficient obtained above, insight into the number of electrons transferred can be achieved through theoretically predicting the peak current using the Randles-Ševčík equation for irreversible electron transfer Eqn. 12. When varying the hydrogen peroxide concentration from 0 to 20 mM, the corresponding peak currents are

measured and compared to the theoretical Randles-Ševčík peak currents. In the experiment, the electrode area of BDDE is 3.7 x 10^{-5} m^2, the scan rate is 0.05 V s^{-1}, the diffusion coefficient is 1.43 x 10^{-9} m^2 s^{-1}, and the transfer coefficient is 0.26. Figure 4 shows the theoretically calculated peak currents based on the above parameters with different values for the number of electrons transferred (n = 2, red and n = 4, green) compared with the experimental peak currents (black). The experimental peak currents show close agreement with the calculated values for a two electron transfer, indicating this to be the likely number of electrons transferred during the process. Note that for this to be true, the layer of oxygen adjacent to the electrode needs to be much greater than the diffusion layer around the electrode during the voltammetric sweep. This condition is set by the time of waiting used in the experiment reported above.

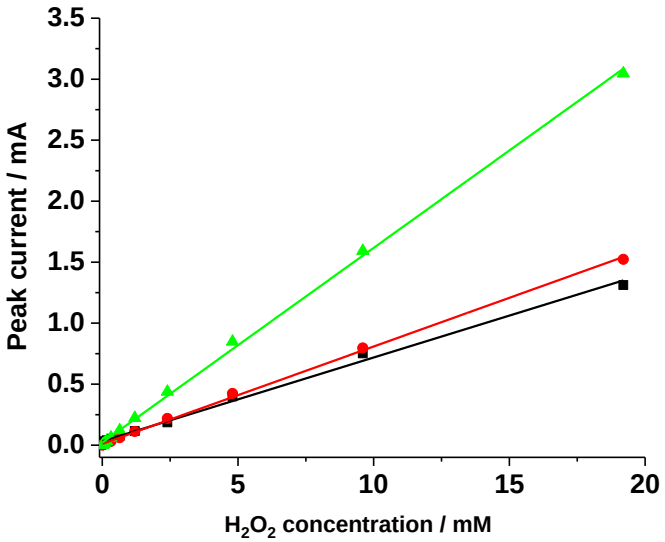

Figure 4. Plots of the experimental (black) and theoretical peak currents (red is n=2, and green is n=4) vs. H_2O_2 concentration.

If the postulated mechanism for the electroreduction of hydrogen peroxide broadly accepted in the literature,[3-7] whereby hydrogen peroxide is first reduced to an adsorbed hydroxide ($OH_{(ads)}$) before being reduced to water (Eqn. 1 and 2), operates, one might expect oxygen reduction to be largely unrelated to the voltammetry produced from hydrogen peroxide. In order to test the mechanism proposed in Eqn. 3 and 4, solutions containing PBS in the *absence* of hydrogen peroxide were saturated with air.

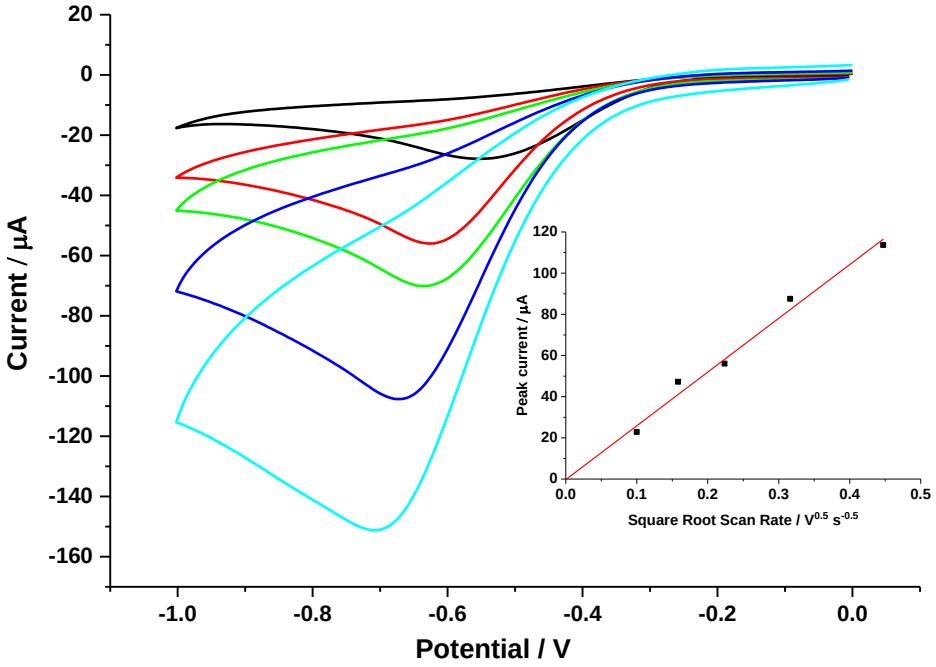

Figure 5. Cyclic voltammogram of AgNPs-BDDE in air-saturated PBS solution at 0.01 V s^{-1} (black), 0.025 V s^{-1} (red), 0.05 V s^{-1} (green), 0.1 V s^{-1} (blue), and 0.2 V s^{-1} (cyan). Inset is the plot of peak current vs square root of the scan rate.

A modified electrode was then immersed in a solution of PBS saturated with air, and a CV was recorded by sweeping the potential from 0.0 V to -1.0 V vs Ag/AgCl. Figure 5 shows the

current response obtained at different scan rates from 0.01 to 0.2 V s^{-1}. In each case, a peak at *ca.* -0.6 – -0.7 V appeared on the forward scan. The plot of peak current versus the square root of scan rate in the inset of Figure 5 is linear, indicating it is a diffusion controlled process.

To characterise the electron transfer process, Tafel analysis for the above process was once again undertaken on the experimental voltammetry (n = 3, Figure S3), and the mean and the errors are listed in Table S2. The mean transfer coefficient, α, was calculated from the Tafel slopes to be 0.28 ± 0.03. The Randles-Ševčík equation for irreversible electron transfers can be once again utilized to predict the theoretical current response, setting $D = 1.96 \times 10^{-9}$ m^2 s^{-1}, and C = 0.26 mM.[30] Figure 6 shows the calculated peak currents (n=2, red and n=4, green) and the experimental peak currents (black). Excellent agreement is observed with the theoretical prediction for the oxygen reduction reaction involving an approximately four electron transfer process, leading to the formation of water. It has been reported that oxygen can be reduced either by a direct 4-electron pathway (Eqn. 13):[38]

$$O_2 + 4H^+ + 4e^- \rightarrow 2H_2O \qquad (13)$$

or by two 2-electron processes (Eqn. 4, reproduced below, and 14) where two electrons are transferred sequentially with hydrogen peroxide production as an oxygen reduction reaction (ORR) intermediate:[1, 2]

$$O_2 + 2e^- + 2H^+ \rightarrow H_2O_2 \qquad (4)$$

$$H_2O_2 + 2H^+ + 2e^- \rightarrow 2H_2O \qquad (14)$$

The first electron transfer to produce the superoxide ion ($O_2^{\bullet -}$) is reported to be the rate determining step.[39]

Furthermore, the kinetics of ORR on silver nanoparticles supported on glassy carbon have been investigated.[15] The voltammetry of ORR was described very satisfactorily with a two-

proton, two-electron reduction process yielding H_2O_2. Moreover, the hydrogen peroxide has been directly detected as an oxygen reduction intermediate for silver electrode using scanning electrochemical microscopy.[40] It demonstrates that the amount of hydrogen peroxide is related to number of electrons transferred and n varies as a function of potential.

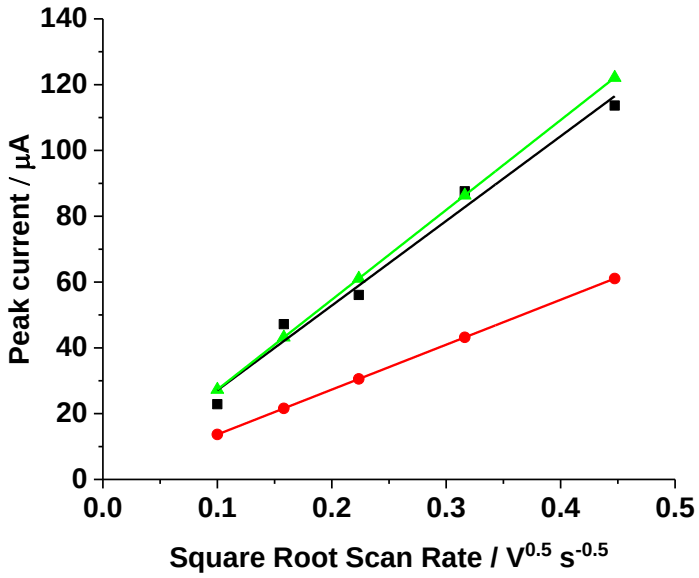

Figure 6. Plot of the experimental (black) and theoretical peak currents (red is n=2, and green is n=4) vs square root scan rate in air-saturated PBS solution.

Having investigated the electron transfer processes for both oxygen and hydrogen peroxide reduction, we next compare these two processes and investigate whether oxygen reduction plays a role in the hydrogen peroxide reduction. Figure 7 shows overlaid experimental voltammograms of oxygen in the absence of hydrogen peroxide (black), and degassed PBS in the presence of different hydrogen peroxide concentrations (0.16 mM (red), 0.32 mM (green), and 0.64 mM (blue)). In terms of waveshape, the voltammograms look very similar, and the

peak potentials of both processes are the same within experimental error, namely E_p = -0.62 ± 0.01 V and E_p = -0.63 ± 0.01 V for hydrogen peroxide and oxygen respectively. Combining this information with the similar transfer coefficient values of 0.26 ± 0.04 and 0.28 ± 0.03 for the reduction of hydrogen peroxide and oxygen reduction respectively, suggests that the electron transfer step in the reduction of hydrogen peroxide plausibly involves oxygen, O_2.

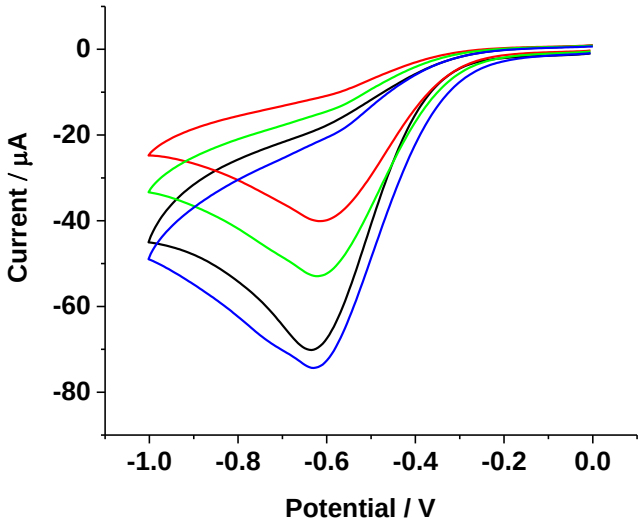

Figure 7. CV recorded on AgNPs-BDDE at a scan rate of 0.05 V s^{-1}. Black is in air-saturated PBS at 0 mM H_2O_2, while others are in N_2-saturated PBS at different H_2O_2 concentrations of 0.16 mM (red), 0.32 mM (green), and 0.64 mM (blue).

To further test the proposed mechanism outlined in Eqn. 3 and 4, a time dependency study was undertaken. The disproportionation of hydrogen peroxide on silver (outlined in Eqn. 3) is relatively slow[15] and so time is required to saturate the diffusion layer adjacent to the electrode. Hence if the suggested mechanism operates, the peak current would be expected to increase with the time that the hydrogen peroxide is in contact with the electrode up to a

limiting value corresponding to a thick layer of O_2 adjacent to the electrode. Not only this, but the wave shape would differ from that observed from an E mechanism. Note that previous investigations of this mechanism neglected to account for any effect of the time, and produced a composite rate constant of $k_0 \exp\left(-\frac{\alpha F E_f}{RT}\right)$ (at presumably long time scales) describing the reduction of H_2O_2 *via* an adsorbed hydroxide intermediate of 0.4 cm s^{-1}.[35]

A modified electrode was submerged into a degassed PBS solution containing 0.32 mM H_2O_2. After a predetermined waiting time (from 5 seconds to 15 minutes), a CV was recorded by sweeping the potential from 0.0 V to -1.0 V vs Ag/AgCl at a scan rate of 0.05 V s^{-1} (Figure 8a). Figure 8b is the plot of average peak current *vs* waiting time. It shows that the peak current increases the longer the electrode is in contact with hydrogen peroxide before the scan is recorded. This indicates the distinct probability of a catalytic decomposition of hydrogen peroxide on the silver surface. As the hydrogen peroxide is chemically decomposed into oxygen, more oxygen accumulates adjacent to the electrode, and it is this oxygen that is then reduced. If hydrogen peroxide was reduced to water (as in Eqn. 14), it would be anticipated that the peak current should be independent of waiting time, further supporting the proposed mechanism in Eqn. 3 and 4.

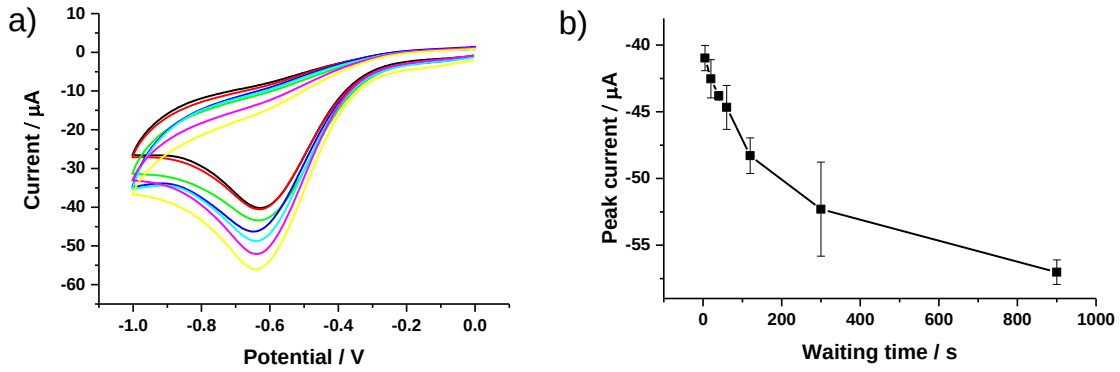

Figure 8. a) CV of AgNPs-BDDE in N_2-saturated PBS containing 0.32 mM H_2O_2 after different interacting time between Ag and H_2O_2 at a scan rate of 0.05 V s^{-1}. Black is 5 s, red 20 s, green 40 s, blue1 min, cyan 2 min, magenta 5 min, and yellow 15 min. b) is the plot of peak current vs waiting time.

To better understand the proposed mechanism, a simulation to the voltammograms in Figure 9 was performed (as detailed in the Theory section). Figure 9 shows the experimental voltammetry (black) compared with simulated voltammetry (red), where the kinetic parameters k_{het}, k_0, and α were optimised to take values of $8x10^{-6}$ m s^{-1}, $1x10^{-7}$ m s^{-1}, and 0.3 respectively, over a range of waiting times t_{wait}. To present the dependence of the reaction current on the waiting time, the currents measured from experiment and calculated from simulation are normalized by the experimental peak current of 900 s t_{wait} and the simulated peak current of 900 s t_{wait}, respectively. It shows in Figure 9 that the simulation fits the time dependence well with above kinetic parameters. The value of k_{het} is approximately one order of magnitude slower than inferred in the literature[15] for significantly larger sized silver nanoparticles, partly suggesting a size effect on the chemical disproportionation reaction.

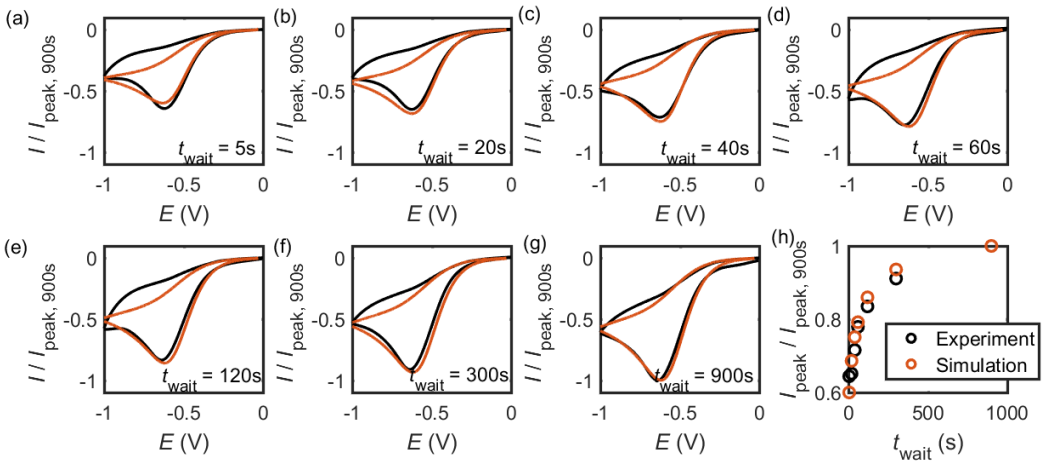

Figure 9 (a)-(g) Cyclic voltammograms from experiment (black) and simulation (red) with various waiting time t_{wait}; (h) Time dependence of the peak currents as a function of waiting time t_{wait}. The experiment and simulation currents are normalized by the experimental and simulated peak currents of the 900s t_{wait}, respectively.

The variance of the peak current with waiting time, and the close resemblance of the voltammetry of oxygen and hydrogen peroxide (both in terms of peak potentials and transfer coefficients), combined with the close agreement of the simulation with the experimental voltammetry provide strong evidence for the reduction of hydrogen peroxide on silver occurring *via* a CE mechanism at neutral pH. This mechanistic insight is likely to prove valuable in the applications of hydrogen peroxide reduction broadly, and represents a significant advancement in our understanding of the electrochemical process.

Conclusions

The reduction of hydrogen peroxide on silver nanoparticle modified BDD electrodes is concluded to follow a CE mechanism, whereby the hydrogen peroxide decomposes to oxygen, and the oxygen is electrochemically reduced to hydrogen peroxide.

Acknowledgements

The research leading to these results has received partial funding from the European Research Council under the European Union's Seventh Framework Programme (FP/2007-2013)/ERC Grant Agreement no. 320403).

References

1. C. M. Welch, C. E. Banks, A. O. Simm and R. G. Compton, *Anal Bioanal Chem*, 2005, **382**, 12-21.
2. S. H. Chen, R. Yuan, Y. Q. Chai and F. X. Hu, *Microchim Acta*, 2013, **180**, 15-32.
3. Z. Y. Chen, C. L. Li, Y. Y. Ni, F. T. Kong, Y. B. Zhang, A. G. Kong and Y. K. Shan, *Electrochim Acta*, 2017, **239**, 45-55.
4. H. Ramezani, S. N. Azizi and S. R. Hosseini, *Sensor Actuat B-Chem*, 2017, **248**, 571-579.
5. N. Zhang, Q. L. Sheng, Y. Z. Zhou, S. Y. Dong and J. B. Zheng, *J Electroanal Chem*, 2016, **781**, 315-321.
6. Q. Wang, S. S. Hu, T. Yang, S. S. Ma, Y. H. Liu, C. X. Ma, M. M. Wan and C. Mao, *J Mater Chem B*, 2017, **5**, 4233-4238.
7. E. Kurowska-Tabor, M. Jaskula and G. D. Sulka, *Electroanal*, 2015, **27**, 1968-1978.
8. H. D. Wang, H. H. Wang, T. F. Li, J. Ma, K. Li and X. Zuo, *Sensor Actuat B-Chem*, 2017, **239**, 1205-1212.
9. L. Y. Jiang, J. P. Hu and J. S. Foord, *Electrochim Acta*, 2015, **176**, 488-496.
10. B. Habibi and M. Jahanbakhshi, *J Iran Chem Soc*, 2015, **12**, 1431-1438.
11. T. R. Bartlett, J. Holter, N. Young and R. G. Compton, *Nanoscale*, 2016, **8**, 13908-13914.
12. L. Mattarozzi, S. Cattarin, N. Comisso, P. Guerriero, M. Musiani and E. Verlato, *Electrochim Acta*, 2016, **198**, 296-303.
13. X. H. Niu, L. B. Shi, J. M. Pan, F. X. Qiu, Y. S. Yan, H. L. Zhao and M. B. Lan, *Electrochim Acta*, 2016, **199**, 187-193.
14. H. Shamkhalichenar and J. W. Choi, *Journal of the Electrochemical Society*, 2017, **164**, B3101-B3106.

15. C. C. M. Neumann, E. Laborda, K. Tschulik, K. R. Ward and R. G. Compton, *Nano Res*, 2013, **6**, 511-524.

16. R. Guidelli, R. G. Compton, J. M. Feliu, E. Gileadi, J. Lipkowski, W. Schmickler and S. Trasatti, *Pure Appl. Chem.*, 2014, **86**, 245-258.

17. R. Guidelli, R. G. Compton, J. M. Feliu, E. Gileadi, J. Lipkowski, W. Schmickler and S. Trasatti, *Pure Appl. Chem.*, 2014, **86**, 259-262.

18. E. J. F. Dickinson, J. G. Limon-Petersen, N. V. Rees and R. G. Compton, *J Phys Chem C*, 2009, **113**, 11157-11171.

19. K. Ngamchuea, S. Eloul, K. Tschulik and R. G. Compton, *Anal Chem*, 2015, **87**, 7226-7234.

20. T. J. Davies, C. E. Banks and R. G. Compton, *J Solid State Electr*, 2005, **9**, 797-808.

21. N. Godino, X. Borrise, F. X. Munoz, F. J. del Campo and R. G. Compton, *J Phys Chem C*, 2009, **113**, 11119-11125.

22. T. J. Davies, S. Ward-Jones, C. E. Banks, J. del Campo, R. Mas, F. X. Munoz and R. G. Compton, *J Electroanal Chem*, 2005, **585**, 51-62.

23. S. R. Belding, F. W. Campbell, E. J. F. Dickinson and R. G. Compton, *Phys Chem Chem Phys*, 2010, **12**, 11208-11221.

24. R. G. Compton, E. Laborda and K. R. Ward, *Understanding Voltammetry: Simulation of Electrode Processes*, Imperial College Press, London, 2014.

25. A. Fick, *J Membrane Sci*, 1995, **100**, 33-38.

26. J. A. V. Butler, *Transactions of the Faraday Society*, 1924, **19**, 729-733.

27. T. Erdey-Grúz and M. Volmer, *Zeitschrift für Physikalische Chemie*, 1930, **150A**, 203-213.

28. S. A. M. van Stroe-Biezen, F. M. Everaerts, L. J. J. Janssen and R. A. Tacken, *Anal Chim Acta*, 1993, **273**, 553-560.

29. K. Shimizu, L. Sepunaru and R. G. Compton, *Chem Sci*, 2016, **7**, 3364-3369.

30. S. V. Sokolov, L. Sepunaru and R. G. Compton, *Applied Materials Today*, 2017, **7**, 82-90.

31. R. G. Compton and C. E. Banks, *Understanding Voltammetry*, Imperial College Press, 2nd edn., 2011.

32. https://www.sigmaaldrich.com/catalog/product/aldrich/730785?lang=en&region=GB

33. P. Gan, J. S. Foord and R. G. Compton, *ChemistryOpen*, 2015, **4**, 606-612.

34. T. J. Cardwell, J. Mocak, J. H. Santos and A. M. Bond, *Analyst*, 1996, **121**, 357-362.

35. F. W. Campbell, S. R. Belding, R. Baron, L. Xiao and R. G. Compton, *J Phys Chem C*, 2009, **113**, 9053-9062.

36. H. S. Toh, C. Batchelor-McAuley, K. Tschulik, M. Uhlemann, A. Crossley and R. G. Compton, *Nanoscale*, 2013, **5**, 4884-4893.

37. S. J. Cloake, H. S. Toh, P. T. Lee, C. Salter, C. Johnston and R. G. Compton, *ChemistryOpen*, 2015, **4**, 22-26.

38. I. Katsounaros, W. B. Schneider, J. C. Meier, U. Benedikt, P. U. Biedermann, A. A. Auer and K. J. J. Mayrhofer, *Phys Chem Chem Phys*, 2012, **14**, 7384-7391.

39. A. J. Appleby, *Journal of the Electrochemical Society*, 1970, **117**, 1373-1378

40. C. M. Sanchez-Sanchez and A. J. Bard, *Anal Chem*, 2009, **81**, 8094-8100.

Graphic Abstract